

Probing New Physics Using Standard Model Effective Field Theory

Anisha*

School of Physics & Astronomy, University of Glasgow, Glasgow G12 8QQ, United Kingdom

E-mail: anisha@glasgow.ac.uk

In the quest for new physics, due to the lack of any direct evidence, the framework of Effective field theory becomes an indirect and consistent way to parametrise NP effects in terms of higher dimension operators. Among the observables with the potential to account for NP signatures, Electroweak Precision Observables and those from Higgs productions and decays play an important role. In this work, we discuss the modifications induced by the Standard Model Effective Field Theory Warsaw basis dimension-6 operators on different observables related to the electroweak sector. We present the model-independent constraints obtained from the global fit performed using the EWPO, single and di-Higgs data, as well as distributions from the di-boson production channels. In addition, we discuss the constraints imposed on the BSM extensions by the considered data via SMEFT matching.

*41st International Conference on High Energy physics - ICHEP2022
6-13 July, 2022
Bologna, Italy*

*Speaker

1. Introduction

The Standard Model Effective Field Theory (SMEFT) parametrises the indirect new physics (NP) effects from the experimental data by connecting the gap between different energy scales. The SMEFT describes any NP in terms of higher-dimensional (mass dimensions ≥ 5) operators consisting of only SM fields and respecting the SM gauge symmetry $SU(3)_C \otimes SU(2)_L \otimes U(1)_Y$. The SMEFT Lagrangian is generalised as:

$$\mathcal{L}_{\text{SMEFT}} = \mathcal{L}_{\text{SM}} + \sum_{d=5,6,\dots} \sum_i \left(\frac{C_i^{(d)}}{\Lambda^{d-4}} \right) Q_i^{(d)}. \quad (1)$$

Here, \mathcal{L}_{SM} is the SM Lagrangian and $Q_i^{(d)}$ are the effective operators of mass dimension d with respective $C_i^{(d)}$ Wilson Coefficients (WCs). The index i runs over the number of independent effective operators, and Λ is the cut-off scale (\gg electroweak scale). We confine our discussion to dimension-6 operators in the Warsaw basis [1] and express the non-SM deviations in the experimental observables in terms of WCs. Using global fits [2–5], we analysed the limits on WCs treated as free and independent. We further matched a BSM scenario to SMEFT and performed BSM-specific fit to constrain BSM parameter space.

The proceeding is outlined as follows: in section 2, we list the observables used in the analysis along with the operators contributing to their SMEFT parametrisations. In section 3, we discuss the global fits and present the model-independent constraints on the SMEFT operators. In section 4, we match a heavy BSM scalar doublet to SMEFT at one-loop and further discuss the bounds on BSM parameters and BSM-specific operators by employing fits using the one-loop matching results and experimental data. Finally, we summarise our results in section 5.

2. Observable datasets and their SMEFT parametrisation

We included the observable datasets comprising Electroweak Precision observables (EWPO) from LEP and Tevatron, LHC single-Higgs data including signal strengths and simplified template cross-section (STXS) measurements from ATLAS and CMS Run-I and II, and for di-Higgs production, the total cross section signal-strength measurements in the $4b$, $2b2\tau$ and $2b2\gamma$ decay channels. We also considered momentum-dependent di-boson distributions (WZ , WW) and the $\Delta\phi_{jj}$ distribution for electroweak Zjj production from ATLAS. For LEP WW data, we considered the cross-section measurements for the process $e^+e^- \rightarrow W^+W^- \rightarrow l\nu l\nu/l\nu qq/qqqq$ at different centre of mass energies and angular distributions. We divide our set of observables into two sets called ‘‘2020 dataset’’ and ‘‘this analysis’’ to highlight the constraining power of the latest measurements. The set called ‘‘this analysis’’ contains updated versions of some experimental analyses and additional data. See Table 1 of Ref. [6] for the full list of the observables. The SMEFT predictions for the observables are computed at linear order in the dimension-6 WCs in the electroweak

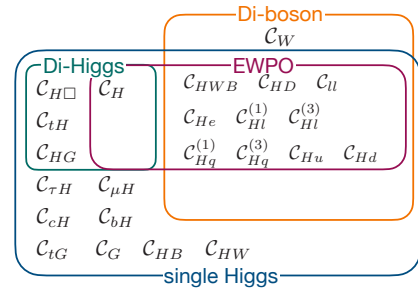


Figure 1: Graphical summary of 23 WCs and the observables they contribute to.

$\{\alpha_{EW}, G_F, m_Z\}$ input scheme with the following input values

$$\alpha_{EW}^{-1} = 127.95, G_F = 1.6638 \times 10^{-5} \text{ GeV}^{-2}, m_Z = 91.1876 \text{ GeV}, m_H = 125.09 \text{ GeV}, m_t = 173.2 \text{ GeV}. \quad (2)$$

In our analysis, 23 WCs contribute to different datasets and the summary of the WCs along with the observables they contribute to is given in Fig. 1. The complete details related to SMEFT predictions are given in section 2 of Ref. [6].

3. Model Independent Analysis

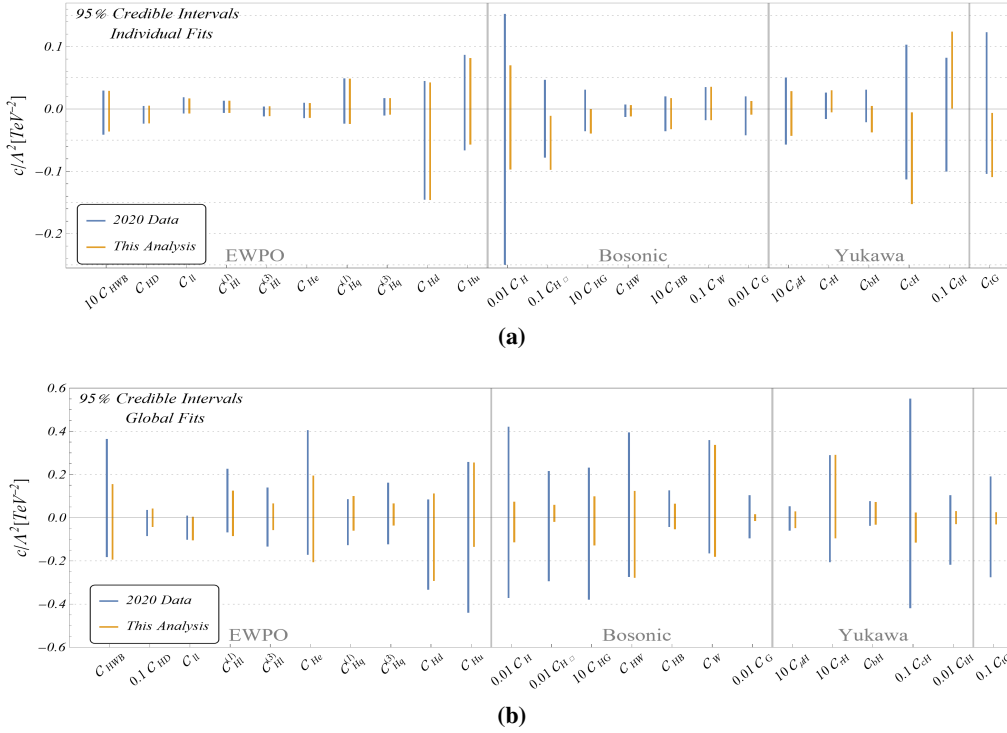


Figure 2: Individual (top) and global (bottom) 95% credible interval (CI) limits on the WCs from fits with the complete dataset (orange) and the reduced set with measurements up to year 2020 (blue).

In this section, we discuss the *bottom-up* approach where SMEFT WCs are treated as free parameters and are constrained using the observable datasets discussed in the previous section. We followed the Bayesian framework to draw the statistical inference, and the parameter estimation is done using the *Mathematica*[®] package *OptEx* [7]. Point estimates are quoted in terms of Medians and fixed quantiles around them. We describe these fits as model-independent, and first, we show the results of one-parameter WCs fits in Fig. 2a. The WCs constrained through EWPO receive much stronger individual bounds than those constrained through Higgs and di-boson observables alone. The most weakly bounded WC is C_H which is most strongly constrained through di-Higgs measurements in our fit. We find that operators constrained via EWPO do not benefit from adding new datasets at the level of one-parameter fits, while on the other hand, the bounds of bosonic as well as Yukawa-like operators are significantly improved. In Fig. 2b, we display the results of our

global fit of 23 WCs after marginalisation. The improvement in the constraints with adding more data appears to be even more significant in the global fit than in the one-parameter fit.

4. Model Dependent Analysis: SM extended with an Extra Scalar Doublet

Now, we discuss *top-down* approach using a BSM scenario of SM extended with an extra heavy isospin-doublet scalar (\mathcal{H}_2) with hypercharge $Y = -\frac{1}{2}$. We integrate out this heavy non-SM doublet using the *Mathematica*[®] package CoDEX [8] incorporating the scalar heavy-light mixing contributions at one-loop. The relevant BSM Lagrangian is

$$\begin{aligned} \mathcal{L}_{\mathcal{H}_2} = & \mathcal{L}_{\text{SM}} + |\mathcal{D}_\mu \mathcal{H}_2|^2 - m_{\mathcal{H}_2}^2 |\mathcal{H}_2|^2 - \frac{\lambda_{\mathcal{H}_2}}{4} |\mathcal{H}_2|^4 \\ & - \lambda_{\mathcal{H}_2,1} |\tilde{H}|^2 |\mathcal{H}_2|^2 - \lambda_{\mathcal{H}_2,2} |\tilde{H}^\dagger \mathcal{H}_2|^2 - \lambda_{\mathcal{H}_2,3} \left[(\tilde{H}^\dagger \mathcal{H}_2)^2 + (\mathcal{H}_2^\dagger \tilde{H})^2 \right]. \end{aligned} \quad (3)$$

Here, $m_{\mathcal{H}_2}$ is the mass of the heavy field and serves as the cut-off scale. After integrating out \mathcal{H}_2 at $m_{\mathcal{H}_2}$ scale (taken as 1 TeV), the complete list of effective operators and accompanying WCs (in terms of BSM parameters) obtained are given in Tab. 1. Furthermore, incorporating these matching results in the SMEFT parametrisations, we discuss the model-specific constraints for three datasets, ‘‘All’’ (blue), ‘‘Higgs’’ (green) and ‘‘EWPO’’ (red) sets of experimental measurements.

Table 1: Warsaw basis dimension-6 effective operators and the associated WCs that emerge after integrating-out the heavy field $\mathcal{H}_2 : (1, 2, -\frac{1}{2})$. Operators highlighted in blue are functions of SM parameters only, while the red coloured ones do not contribute to our observables.

Operators	Wilson coefficients	Operators	Wilson coefficients	Operators	Wilson coefficients
Q_{dH}	$\frac{\lambda_{\mathcal{H}_2,2}^2 Y_{d,2}^{\text{SM}}}{192\pi^2 m_{\mathcal{H}_2}^2} + \frac{\lambda_{\mathcal{H}_2,3}^2 Y_{d,3}^{\text{SM}}}{48\pi^2 m_{\mathcal{H}_2}^2}$	$Q_{Hq}^{(1)}$	$-\frac{g_Y^4}{11520\pi^2 m_{\mathcal{H}_2}^2}$	Q_{ee}	$-\frac{g_Y^4}{1920\pi^2 m_{\mathcal{H}_2}^2}$
Q_{eH}	$\frac{\lambda_{\mathcal{H}_2,2}^2 Y_{e,2}^{\text{SM}}}{192\pi^2 m_{\mathcal{H}_2}^2} + \frac{\lambda_{\mathcal{H}_2,3}^2 Y_{e,3}^{\text{SM}}}{48\pi^2 m_{\mathcal{H}_2}^2}$	Q_{Hd}	$\frac{g_Y^4}{5760\pi^2 m_{\mathcal{H}_2}^2}$	Q_{eu}	$\frac{g_Y^4}{1440\pi^2 m_{\mathcal{H}_2}^2}$
Q_{uH}	$\frac{\lambda_{\mathcal{H}_2,2}^2 Y_{u,2}^{\text{SM}}}{192\pi^2 m_{\mathcal{H}_2}^2} + \frac{\lambda_{\mathcal{H}_2,3}^2 Y_{u,3}^{\text{SM}}}{48\pi^2 m_{\mathcal{H}_2}^2}$	Q_{He}	$\frac{g_Y^4}{1920\pi^2 m_{\mathcal{H}_2}^2}$	Q_{uu}	$-\frac{g_Y^4}{4320\pi^2 m_{\mathcal{H}_2}^2}$
Q_H	$-\frac{\lambda_{\mathcal{H}_2,1}^3}{48\pi^2 m_{\mathcal{H}_2}^2} + \frac{\lambda_H^{\text{SM}} \lambda_{\mathcal{H}_2,2}^2}{96\pi^2 m_{\mathcal{H}_2}^2} - \frac{\lambda_{\mathcal{H}_2,1}^2 \lambda_{\mathcal{H}_2,2}}{32\pi^2 m_{\mathcal{H}_2}^2}$ $-\frac{\lambda_{\mathcal{H}_2,1} \lambda_{\mathcal{H}_2,2}^2}{32\pi^2 m_{\mathcal{H}_2}^2} + \frac{\lambda_H^{\text{SM}} \lambda_{\mathcal{H}_2,3}^2}{24\pi^2 m_{\mathcal{H}_2}^2} - \frac{\lambda_{\mathcal{H}_2,2}^3}{96\pi^2 m_{\mathcal{H}_2}^2}$ $-\frac{\lambda_{\mathcal{H}_2,1} \lambda_{\mathcal{H}_2,3}^2}{8\pi^2 m_{\mathcal{H}_2}^2} - \frac{\lambda_{\mathcal{H}_2,2} \lambda_{\mathcal{H}_2,3}^2}{8\pi^2 m_{\mathcal{H}_2}^2}$	Q_{Hu}	$-\frac{g_Y^4}{2880\pi^2 m_{\mathcal{H}_2}^2}$	Q_{lu}	$\frac{g_Y^4}{2880\pi^2 m_{\mathcal{H}_2}^2}$
$Q_{H\Box}$	$-\frac{g_W^4}{7680\pi^2 m_{\mathcal{H}_2}^2} - \frac{\lambda_{\mathcal{H}_2,1}^2}{96\pi^2 m_{\mathcal{H}_2}^2}$ $-\frac{\lambda_{\mathcal{H}_2,1} \lambda_{\mathcal{H}_2,2}}{96\pi^2 m_{\mathcal{H}_2}^2} + \frac{\lambda_{\mathcal{H}_2,3}^2}{48\pi^2 m_{\mathcal{H}_2}^2}$	$Q_{Hl}^{(3)}$	$-\frac{g_Y^4}{1920\pi^2 m_{\mathcal{H}_2}^2}$	Q_{qe}	$\frac{g_Y^4}{5760\pi^2 m_{\mathcal{H}_2}^2}$
Q_{HD}	$-\frac{g_Y^4}{1920\pi^2 m_{\mathcal{H}_2}^2} - \frac{\lambda_{\mathcal{H}_2,2}^2}{96\pi^2 m_{\mathcal{H}_2}^2} + \frac{\lambda_{\mathcal{H}_2,3}^2}{24\pi^2 m_{\mathcal{H}_2}^2}$	$Q_{Hq}^{(3)}$	$-\frac{g_W^4}{1920\pi^2 m_{\mathcal{H}_2}^2}$	Q_{ld}	$-\frac{g_Y^4}{5760\pi^2 m_{\mathcal{H}_2}^2}$
Q_{HB}	$\frac{g_Y^2 \lambda_{\mathcal{H}_2,1}}{384\pi^2 m_{\mathcal{H}_2}^2} + \frac{g_Y^2 \lambda_{\mathcal{H}_2,2}}{768\pi^2 m_{\mathcal{H}_2}^2}$	Q_W	$\frac{g_W^3}{5760\pi^2 m_{\mathcal{H}_2}^2}$	$Q_{qq}^{(1)}$	$-\frac{g_Y^4}{69120\pi^2 m_{\mathcal{H}_2}^2}$
Q_{HW}	$\frac{g_W^2 \lambda_{\mathcal{H}_2,1}}{384\pi^2 m_{\mathcal{H}_2}^2} + \frac{g_W^2 \lambda_{\mathcal{H}_2,2}}{768\pi^2 m_{\mathcal{H}_2}^2}$	Q_{ll}	$-\frac{g_W^4}{7680\pi^2 m_{\mathcal{H}_2}^2} - \frac{g_Y^4}{7680\pi^2 m_{\mathcal{H}_2}^2}$	Q_{le}	$-\frac{g_Y^4}{1920\pi^2 m_{\mathcal{H}_2}^2}$
Q_{HWB}	$\frac{g_W g_Y \lambda_{\mathcal{H}_2,2}}{384\pi^2 m_{\mathcal{H}_2}^2}$	$Q_{ud}^{(1)}$	$\frac{g_Y^4}{4320\pi^2 m_{\mathcal{H}_2}^2}$	$Q_{qd}^{(1)}$	$\frac{g_Y^4}{17280\pi^2 m_{\mathcal{H}_2}^2}$
$Q_{Hl}^{(1)}$	$\frac{g_Y^4}{3840\pi^2 m_{\mathcal{H}_2}^2}$	$Q_{lq}^{(3)}$	$-\frac{g_W^4}{3840\pi^2 m_{\mathcal{H}_2}^2}$	$Q_{qu}^{(1)}$	$-\frac{g_Y^4}{8640\pi^2 m_{\mathcal{H}_2}^2}$
		$Q_{qq}^{(3)}$	$-\frac{g_W^4}{7680\pi^2 m_{\mathcal{H}_2}^2}$	$Q_{lq}^{(1)}$	$\frac{g_Y^4}{11520\pi^2 m_{\mathcal{H}_2}^2}$
		Q_{dd}	$-\frac{g_Y^4}{17280\pi^2 m_{\mathcal{H}_2}^2}$		
		Q_{ed}	$-\frac{g_Y^4}{2880\pi^2 m_{\mathcal{H}_2}^2}$		

Constraints on the model parameters

To bound the BSM parameters using the experimental data and SMEFT, the operators coloured in black and blue in Tab. 1 are replaced by the corresponding WCs in the SMEFT parametrisation of the observables. Using OptEx, we perform the fits and show the results as two-dimensional marginal posteriors in Fig. 3. Constant-probability-contours enclose respectively 68% (blue solid, red/green dashed) and 95% (blue dot-dashed, red/green dotted) credible regions. Coloured contours (blue/red/green) with variable-density-shading (darker to lighter) indicate regions of high probability. We find that the constraints from Higgs data are slightly stronger overall, and EWPO data add orthogonal information, leading to significantly tightened bounds when combining the measurements from both sectors.

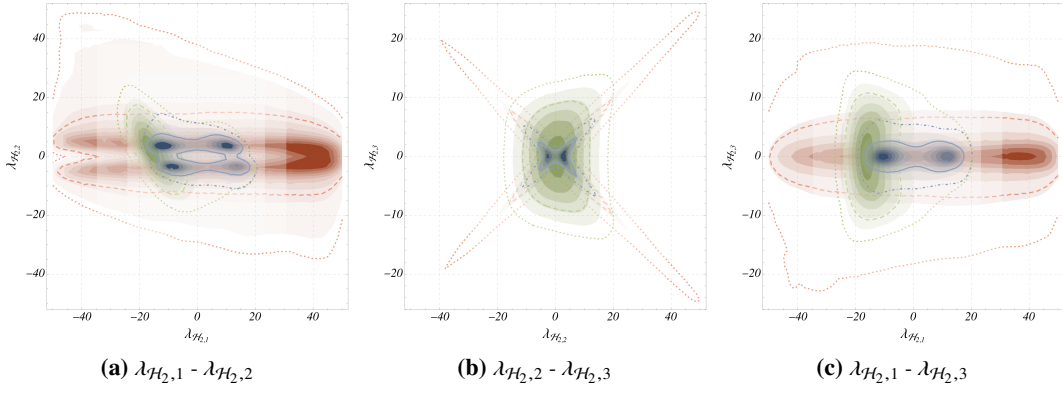


Figure 3: Two-dimensional marginalised posteriors among the BSM parameters. The line contours represent the 68% and 95% credible intervals (CIs) and the filled contours with changing opacity show the high-probability regions with decreasing probabilities (darker to lighter). We show these results from a fit of “EWPO” data only (red), “Higgs” data only (green) as well as for “All” (blue).

Model-Dependent constraints on the WCs

We generate the allowed distributions of BSM-specific WCs (black) using the non-linear relations (obtained after matching) from Tab. 1 expressed in terms of parameters: $\lambda_{H_2,1}$, $\lambda_{H_2,2}$ and $\lambda_{H_2,3}$, and propagating the model-parameter-posteriors (Figs. 3a-3c). Instead of showing all the possible 2D-marginal contour-plots for the WCs¹, we choose to show a few sample plots in Fig. 4.

5. Conclusions

We performed a global fit of 23 Wilson coefficients using datasets comprising Higgs and di-boson sectors plus electroweak precision observables. Our fit includes di-Higgs measurements for the first time, which improves the bounds on a modified Higgs potential through C_H . With the addition of the latest STXS measurements up to high energies, the limits on operators describing Higgs-top and Higgs-gluon interaction are strengthened by up to a factor of 9 compared to previous analyses. We further matched a heavy BSM doublet to SMEFT at one-loop level and obtained the operators and WCs (in terms of BSM parameters). We used the matching expressions and

¹All the relevant WCs plots are given in the Github repository [\[1\]](#).

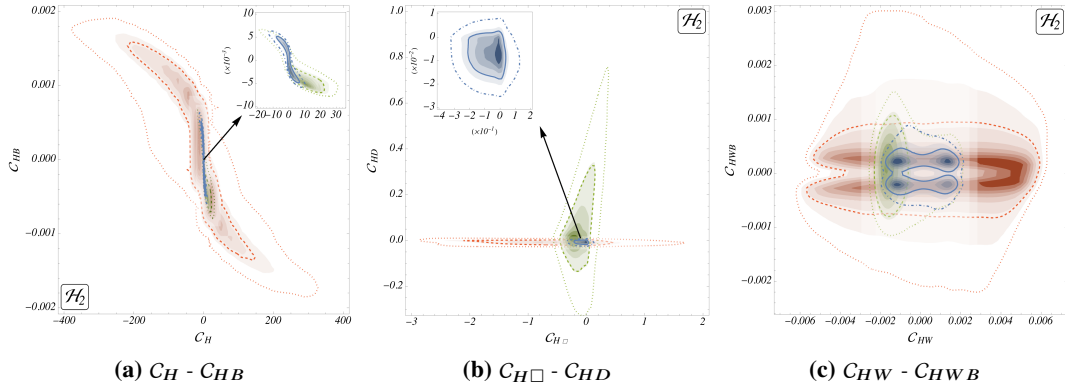


Figure 4: Two-dimensional posteriors among the relevant WCs induced by \mathcal{H}_2 , listed in black in tab. 1. The line contours represent the 68% and 95% CIs and the filled contours with changing opacity denote the high-probability regions with decreasing probabilities (darker to lighter). These allowed regions are shown from fits of “EWPO” data (red), “Higgs” data only (green) and “All” data (blue).

datasets to constrain the BSM parameters. We also highlighted the individual impact of different datasets (EWPO and Higgs data) through two-dimensional posteriors in the model parameter and WC spaces. We studied the impact on the parameter constraints by including Renormalisation group equations; for full details see [6].

References

- [1] B. Grzadkowski, M. Iskrzynski, M. Misiak and J. Rosiek, *Dimension-Six Terms in the Standard Model Lagrangian*, *JHEP* **10** (2010) 085, [[1008.4884](#)].
- [2] J. Ellis, M. Madigan, K. Mimasu, V. Sanz and T. You, *Top, Higgs, Diboson and Electroweak Fit to the Standard Model Effective Field Theory*, *JHEP* **04** (2021) 279, [[2012.02779](#)].
- [3] Anisha, S. Das Bakshi, J. Chakraborty and S. K. Patra, *Connecting electroweak-scale observables to BSM physics through EFT and Bayesian statistics*, *Phys. Rev. D* **103** (2021) 076007, [[2010.04088](#)].
- [4] S. Dawson, S. Homiller and S. D. Lane, *Putting standard model EFT fits to work*, *Phys. Rev. D* **102** (2020) 055012, [[2007.01296](#)].
- [5] SMEFT collaboration, J. J. Ethier, G. Magni, F. Maltoni, L. Mantani, E. R. Nocera, J. Rojo et al., *Combined SMEFT interpretation of Higgs, diboson, and top quark data from the LHC*, *JHEP* **11** (2021) 089, [[2105.00006](#)].
- [6] Anisha, S. Das Bakshi, S. Banerjee, A. Biekötter, J. Chakraborty, S. Kumar Patra et al., *Effective limits on single scalar extensions in the light of recent LHC data*, [2111.05876](#).
- [7] S. Patra, *sunandopatra/optex-1.0.0: Wo documentation*, <https://doi.org/10.5281/zenodo.3404311>, Sept., 2019. 10.5281/zenodo.3404311.
- [8] S. Das Bakshi, J. Chakraborty and S. K. Patra, *CoDEx: Wilson coefficient calculator connecting SMEFT to UV theory*, *Eur. Phys. J. C* **79** (2019) 21, [[1808.04403](#)].